Reprinted by permission from
IEEE JOURNAL OF QUANTUM ELECTRONICS
Vol. QE-9, No. 8, August 1973

A Study of the CW 28-μm Water-Vapor Laser

EARL R. MOSBURG, JR.

Abstract—**The low signal gain of a CW water-vapor laser at 28 μm was measured as a function of the discharge current and pressure. Together with the measurement of other quantities such as the axial electric field and the concentration of OH, a partial interpretation of the mechanisms involved in pumping the 28-μm transition was possible. Thermal equilibrium between the ν_0, $2\nu_2$, and ν_3 vibrational levels will result in a large absorption at the elevated gas temperatures observed (800–1000 K). The strong dependence of gain on the electron temperature strongly suggests that the vibrational excitation proceeds through electron-impact excitation. Only the electron-impact excitation of H_2O is quantitatively capable of overcoming the large thermally induced absorption. Although vibrational-excitation transfer from H_2 to H_2O seems insufficient, by itself, to overcome this absorption, it may provide appreciable additional gain. Pumping of the 28-μm line through electron–ion recombination and by reactions involving OH can be ruled out.**

I. Introduction

THE operation of the H_2O far infrared laser, discovered in 1964 by Crocker *et al.* [1], is still not well understood. Although the lasing levels have been identified by Benedict *et al.* [2] as those of the ground-state water molecule and several studies have been made of the pulsed H_2O laser [3], [4], the exact mechanisms involved in producing the population inversion are still uncertain. There are very definite differences between the pulsed and steady-state H_2O lasers, the former operating on many more lines than the steady-state laser. This may be simply a result of the nonequilibrium conditions in the pulsed discharge, or may indicate the presence of additional mechanisms due to the much higher instantaneous excitation power applied in the pulsed case.

In an attempt to delimit the problem, this paper is confined to studies of the brightest line of the CW pure H_2O laser, the 28-μm radiation coupling the $\nu_3 6_{33}$ and the $2\nu_2 5_{50}$ levels [2]. This case has not hitherto been studied in any great detail. Continuous emission at 28 μm has been observed at powers as high as 400 or 500 mW [5][1] from a 37-mm diameter 8-m-long tube. Taking into account the active volume ($\approx 5.6 \times 10^3$ cm^3) of the laser beam, this yields a power density of $\sim$70–90 μW·cm^{-3} or a 28-μm laser photon production density of $\sim 10^{16}$ photons cm^{-3} s^{-1}.

An obvious candidate for explaining the population inversion is excitation by hot electrons. Evidence has been presented that this is, in some form, the major mechanism in the pulsed H_2O laser [4]. However, this does not necessarily rule out the importance of other mechanisms

Manuscript received February 26, 1973; revised April 10, 1973. Contribution of the National Bureau of Standards, not subject to copyright.

The author is with the Quantum Electronics Division, National Bureau of Standards, Boulder, Colo. 80302.

[1] The laser used a partially transmitting silicon output mirror and operated with an H_2O–H_2 mixture.

in the steady-state laser. The possible mechanisms which were considered in this paper are listed below.

A) Excitation of H_2O by hot electrons, either directly to the upper vibrational level of the lasing transition or by relaxation from higher vibrational levels. This may be either by direct dipole interaction or through the formation of an intermediate negative ion state.

B) Vibrational excitation transfer from electron-impact excited H_2 to neutral H_2O in the near resonant reaction [6]

$$H_2(v = 1) + H_2O \rightarrow H_2(v = 0) + H_2O(001). \quad (1)$$

Vibrational excitation transfer from OH to H_2O is also considered.

C) Ionization of neutral H_2O followed by recombination of the resulting H_3O^+ ion and its hydrates. A fair fraction of the 6.45-eV excess energy of recombination may be left in vibrational excitation.

D) Chemical reactions, particularly involving OH as in the reaction

$$H_2 + OH \xrightarrow{k_L} H + H_2O + 0.66 \text{ eV}. \quad (2)$$

Such an H-transfer reaction may leave the resultant H_2O with the required asymmetric-stretch vibrational energy.

In the positive column the ionization source term is provided by the high-energy tail of the electron-velocity distribution, the predominant mechanism being the direct production of H_2O^+ by electron impact. Dissociative ionization producing H^+ and OH^+ is considerably less likely [7]. Following the production of H_2O^+, a very rapid reaction having essentially 100-percent probability per collision [8] transforms H_2O^+ to H_3O^+ in collisions with H_2O. The ionic composition of the discharge is further modified by reversible hydration reactions involving collisions with H_2O. The final result of these three groups of reactions is that the dominant ions of the water-vapor positive column are H_3O^+ and its hydrates.

The dominant loss mechanism for the ions (except near the wall of the discharge tube) is electron–ion recombination, which necessarily leads to dissociation. The measured recombination coefficients determined for these reactions at 540 K are [9] $\alpha(H_3O^+) = 1.1 \times 10^{-6}$ cm^3 s^{-1} and $\alpha(H_3O^+ \cdot H_2O) = 2.4 \times 10^{-6}$ cm^3 s^{-1}.

II. The Experimental Results

A major difficulty in studying the steady-state water-vapor laser was the limited number of parameters that were accessible to measurement. The general types of measurement which were performed are listed below:

1) gain measurements and laser-power measurements;
2) plasma properties: n_e and T_e, and axial electric field;
3) spectroscopy: emission in visible and infrared, and absorption by OH;
4) mass spectroscopy of positive ions from the discharge;
5) effects of impurities: titration chemistry;
6) time-dependent measurements of some of the above.

Brief descriptions of these measurements will now be given. Other experimental results will be introduced where needed in the analysis.

Gain measurements were made by passing the 28-μm radiation from a 4-m-long 59-mm-bore beam-splitter coupled water-vapor laser through a gain tube with polyethylene windows, and monitoring the power received at a triglycinesulfate (TGS) pyroelectric detector for both on and off conditions of the discharge in the gain tube. The on currents varied from about 50 mA to 500 mA for pressures of 0.1 to several torr (1 torr $\cong$ 133 Pa). In the off condition a trickle current of approximately 3–10 mA was maintained to facilitate returning to the on condition. Care was taken to be sure no residual gain was present in the off condition.

Contour maps of the gain versus the water-vapor pressure and gain-tube current were thus determined for nine gain tubes of various inside diameters ranging from 59 mm down to 4.2 mm. The 28-μm beam was chopped, where the beam emerged from the H_2O laser, at a rate of approximately 40 Hz, this frequency then being used as a reference for the synchronous detection of the output of the pyroelectric detector. The amplitude of this detected and filtered signal was converted to a pulse rate in a voltage–frequency converter which was then fed through gate circuits to two scalers accumulating counts for the on and off conditions. The circuit was arranged in such a manner that a waiting time of approximately 1 s was introduced after changing the gain tube from off to on conditions, or vice versa, in order to eliminate transient gain behavior. The integration of data on the two scalers for approximately 15 s each allowed the determination of a gain as small as $\sim \pm 0.1$ percent.

The resulting gain maps, shown in Figs. 1 and 2 for the most thoroughly studied tubes, illustrate the way in which the gain "hill" changes as we go to smaller bore tubes. For the larger bore tubes the gain maximum is a ridge running parallel to and near the current axis with no well-defined peak. As smaller bore tubes are used, this ridge moves away from the current axis, rotates clockwise, and develops a distinct peak in gain which becomes higher for the smaller tubes. For large-bore tubes the gain ridge drops progressively to the right into a region of high absorption. As the bore is decreased, the boundary between gain and absorption regions becomes more convoluted, with the regions of absorption overlying and partially underlying the gain peak. For the smallest bore tube studied, the gain peak is very close to the pressure axis of the plot. This tube was very difficult to modulate as the discharge frequently went out and the trickle current needed to maintain the discharge produced a nonnegligible gain. Table I presents the parameters of the gain tubes and the operating conditions for the case of maximum gain in each tube. These results are plotted in Fig. 3. The gain and the H_2O pressure both follow a curve inversely proportional to the bore radius R, suggesting that the increase in gain is directly related to the increased H_2O pressure in the gain

TABLE I

VALUES OF THE GAIN-TUBE PARAMETERS FOR MAXIMUM GAIN CONDITIONS IN VARIOUS BORE-DIAMETER TUBES

Tube bore [mm]	Tube length [m]	p [torr]	I [A]	V probe [V]	G [% m^{-1}]	Gas Temperature [K]	N [10^{16} cm^{-3}]	E/N [10^{-15} V·cm^2]	n_e [10^{10} cm^{-3}]
59.0	3.5	0.33	0.4	2600	0.7	1020	0.31	2.4	0.76
51.5	1.8		0.35		1.0				
34.0	0.91	0.5	0.35	710	2.3	970	0.55	1.42	2.94
25.4	0.91	0.65	0.30	(800)	2.1	960	0.75	1.17	5.40
19.0	0.91	1.1	0.24	1310	2.3	1080	1.13	1.28	7.06
12.7	0.90	1.5	0.18	1780	4.7	1090	1.6	1.24	12.2
9.5	0.90	1.7	0.14	1960	6.6	1020	2.4	0.91	25.6
6.3	0.90	~3+	0.11	(~3500)	7.2	~1175	4.9	0.8	59.5
4.2	0.91	~4+	0.05	(~4000)	>8.8	~900			

Note: Values in parentheses are estimates or interpolations.

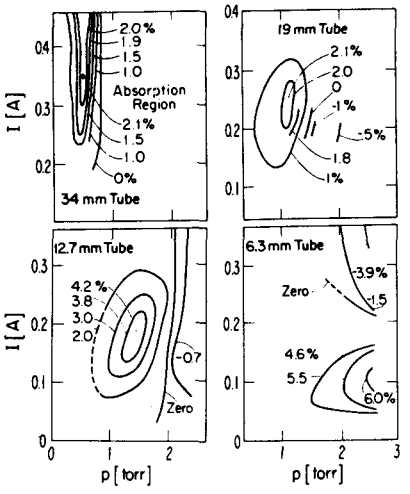

Fig. 1. Contour maps of the measured gain versus the discharge current and water-vapor pressure (measured during the off condition) for gain tubes for four different bore diameters. The gain tubes are all either 90 or 91 cm in length.

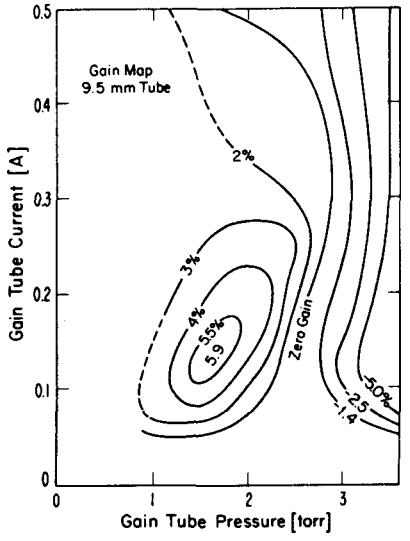

Fig. 2. Contour map of the measured gain versus the discharge current and water-vapor pressure (measured during the off condition) for a 9.5-mm-bore gain tube 90 cm long.

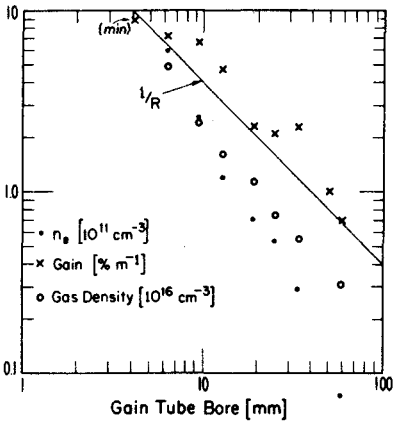

Fig. 3. Various parameters of the gain tubes measured at the optimum (peak-gain) conditions for each tube and plotted versus the bore diameter for each tube. The data are taken from Table I.

tube. The electron density varies even more rapidly with R, $\propto 1/R^{1.8}$, but E/N (and hence the electron temperature) seems to be slightly higher for the larger tubes. The analysis used to obtain these results will be discussed later in the paper.

The major plasma parameters of electron density n_e and temperature T_e were determined in the 59-mm-bore tube, the former by a microwave interferometer at 35 GHz and the latter by Langmuir-probe measurements. Typical values for the operating conditions of this tube were $n_e \cong 1.5\text{–}2 \times 10^{10}$ cm^{-3} and $kT_e \cong 2.4$ eV($T_e \cong 28\,000$ K). The observed time dependence of n_e after plasma excitation is removed yields values for the recombination coefficient consistent with those of Biondi [9]. In addition, the axial electric field was determined by measuring the floating potential of a Langmuir probe placed at the entrance of the gain tube. Since the axial field is known to be essentially constant along the positive column and since the discharge was operated with a grounded anode close to the end of the gain tube, the axial field E could then be calculated by dividing the floating-probe potential by the length of the gain tube. The significance of these measurements will be discussed later.

Spectroscopic studies were hampered by the paucity of lines giving any pertinent information. The visible and near-visible portion of the spectrum is dominated by the emission of atomic hydrogen and of the bright $A^2\Sigma^+ - X^2\Pi(v = 0 \rightarrow 0)$ electronic rotational band of OH at 3064 Å. High-resolution studies of this band were made in order to determine the rotational temperature, which under some conditions [4] can be related to the neutral gas temperature. Optical absorption measurements were made on this band at 3090 Å using the oscillator strength of Bird and Schott [10] in order to determine the concentration of the OH radical and its time dependence as the discharge is switched on and off. For the 59-mm-bore tube under optimum conditions the resulting value was $[OH] \sim 2 \times 10^{12}$ cm^{-3}.

Although the 2.7-μm band of H_2O ($\nu_3 \rightarrow \nu_0$) was detected and monitored in emission with IR interference filters and large solid angles, the power of $\sim 3 \times 10^{-8}$ W at the PbS detector from a 100-cm^3 volume of the discharge was so low that it was not possible to analyze the band through an $f/8$ spectrometer with its inherently small solid angle. Although the minimum detectable power was lowered to $<10^{-11}$ W for an integration time of 30 s, not even the brightest lines in the 2.7-μm band could be detected. Since the lines of greatest interest are much weaker, attempts in this direction were soon abandoned. The photon-emission density in the 2.7-μm band, $\approx 4 \times 10^9$ cm^{-3} s^{-1}, can be related to the population density of the ν_3 vibrational state by using the published line strengths [11]. The result is a value $[H_2O(\nu_3)] \approx 0.7 \times 10^{13}$ cm^{-3}.

III. Analysis of the Gain Contour Maps

Measurements of the voltage drop across the gain tube, together with the gain-tube pressure and current, enable a rough reconstruction of the discharge conditions within the gain tube during the gain measurements. The parameters we would like to know but cannot measure directly for the small-bore tubes are the H_2O gas temperature, the normalized axial electric field E/N, the electron temperature; and the electron density. The 9.5-mm-ID gain tube was chosen for a detailed analysis of these parameters.

The neutral gas temperature T was calculated by balancing the total power input per unit length $P = EI$ against the thermal conduction to the wall through the water vapor. Assuming a Bessel-function distribution for the electron density, then the current density $J(r)$ is given by

$$J(r) = J(0)\, J_0(2.404r/R).$$

Using $x \equiv 2.404r/R$, the thermal-power input within a radius r inside the gain tube can be written as

$$P(x) = 2\pi\Lambda^2 E J(0) \int_0^x J_0(x)\, dx = 2\pi\Lambda^2 E J(0) x J_1(x)$$

where $\Lambda \equiv R/2.404$ is the usual diffusion-length parameter. This power input is then balanced by the thermal conduction loss $-\lambda(T)(dT/dx)2\pi x$ where the thermal conductivity λ is a function of the gas temperature given approximately by $\lambda(T) = 1.8 \times 10^{-4}(T/300)^{1.35}$ W·cm^{-1}·K^{-1} [12]. When $r = R$ we obtain for the total input power the expression $P = EI = P(2.404) = 7.85\Lambda^2 EJ(0) = 1.36R^2 J(0)E$. The heat-balance equation can then be written in the form

$$-\lambda(T)dT = J_1(x)\, dx \cdot P/7.86$$

which integrates giving an axial gas temperature of

$$T = 300\,(1+5.5P)^{0.428} \qquad (3)$$

where P is in units of watts per centimeter. A contour map of the calculated neutral temperature versus p and I for the 9.5-mm-ID gain tube is shown in Fig. 4.

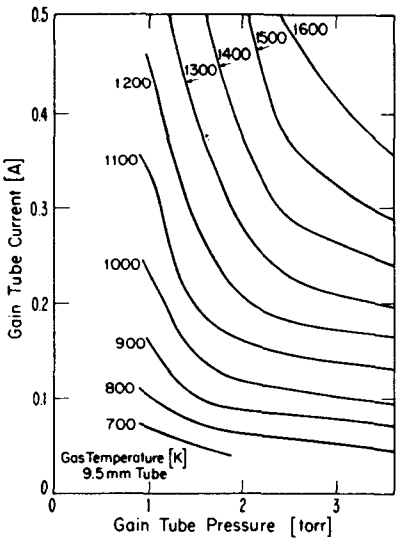

Fig. 4. Contour map of the gas temperature in degree Kelvin calculated from (3) for the 9.5-mm-diameter gain tube.

Partial corroboration of the elevated gas temperatures was obtained in three ways. Measurements were made, in the 9.5-mm tube, of the rotational temperature of several bands of the electronic transition in $OH(v = 0 \rightarrow 0)$ at 3064 Å. An analysis was made for the Q_1, P_1, R_1, and R_2 branches which yielded temperatures ranging from 530 to 1000 K. The P_1 branch, which seemed to have less scatter from line to line, gave temperatures from 810 to 1000 K under conditions when the calculated gas temperatures would be from 1000 to 1330 K. Here, lines out to K = 8 or 9 could be used. There was, however, no correlation between the measured and calculated temperatures.

Secondly, in the H_2O laser tube (ID 59 mm) measurements of relative ion concentrations with the sampling mass spectrometer under typical lasing conditions indicated a ratio mass 37 to mass 19 of about unity. The equilibrium ratios of the different hydrated ions have been measured by Kebarle *et al.* [13] as a function of gas temperature and pressure. Using their results we can convert the measured ion-intensity ratio to a gas temperature of approximately 740 K. The temperature calculated from the input power by (3) is 910 K.

Finally, an upper limit to the temperature can be calculated by assuming collisional equilibrium between the ν_3 and ν_0 vibrational states and using the value of

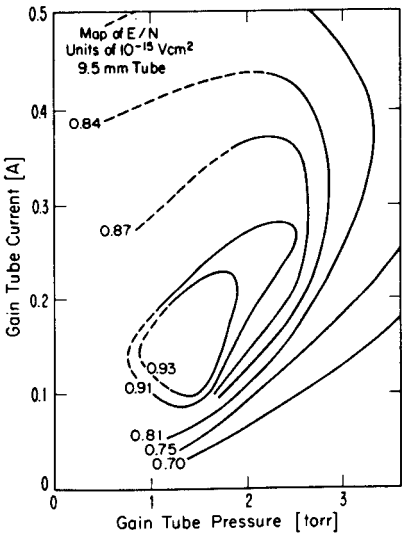

Fig. 5. Contour map of E/N calculated from the measured potential drop across the length of the 9.5-mm gain tube using values of N from (4).

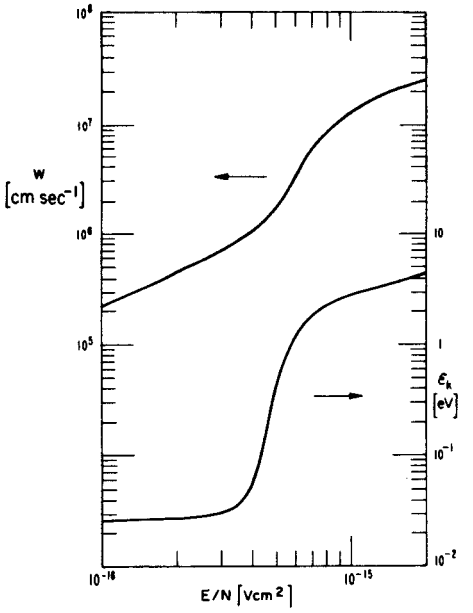

Fig. 6. Relationship between E/N, the characteristic energy ε_k, and the drift velocity w, for a pure H_2O discharge with the neutral gas at room temperature. The data are that of Phelps [14].

$[H_2O(\nu_3)] \simeq 7 \times 10^{12}$ cm^{-3} derived above from the measured 2.7-μm band emission. To the extent that some of the measured density in the ν_3 level is due to the electron-impact excitation, the thermal contribution and, hence, the calculated neutral temperature will be lower. The calculated maximum temperature is then 910 K compared with 1020 K obtained from (3). Although this last discrepancy would be resolved if the ratio of ν_3/ν_0 densities was higher by a factor of only 1.7, it is still possible overall that the calculation of the gas temperature from the power input may be too high by 10 or 20 percent.

In order to calculate E/N values for different operating conditions, we need to correct for both pressure and temperature variations. Since the pressure p denoted by the abscissa of the contour maps is the pressure under discharge off conditions, the actual gas density N present during the discharge will be given by

$$N = N_0 p \frac{300 p^*}{T p} \tag{4}$$

where N_0 is the neutral density, 3.22×10^{16} molecules torr^{-1} cm^{-3} at a temperature of 300 K, and p^*/p is the ratio of pressure for discharge on/discharge off conditions. Measurements of this pressure ratio were made for a few values of p and I. Since no correlation exists between the measured p^*/p and the calculated values of T, the best procedure is to use a median value, $p^*/p = 1.5$. The extrema of the measured pressure ratios then lie within a factor 1.34 of this value. The values of E/N can then be calculated and result in the contour map shown in Fig. 5. The similarity between this figure and the gain contour map, Fig. 2, is very significant.

Since the value of E/N is related monotonically to the mean electron energy, this indicates immediately that the inversion mechanism is controlled by the electron temperature. Unpublished results of Phelps and Cohen [14] allow one to estimate the electron temperature, assuming that the electron-energy distribution is Maxwellian. Thus Fig. 6 shows the calculated relations between E/N and the characteristic energy ε_k (the ratio of the electron-diffusion coefficient to the mobility), which for a Maxwellian distribution is equal to kT_e. The value (at maximum gain) of $E/N = 0.91 \times 10^{-15}$ V·cm^2 then corresponds to a value, $kT_e = 2.7$ eV. In the 59-mm tube under lasing conditions, Langmuir-probe measurements showed a near-Maxwellian distribution with $kT_e = 2.4$ eV. Again comparing Figs. 2 and 5, the contour of zero gain corresponds to $E/N \simeq 0.84 \times 10^{-15}$ V·cm^2, or $kT_e \simeq 2.4$ eV. In the region of lower E/N, particularly where $p = 3.5$ torr and $0.05 < I < 0.1$ A in Fig. 2, we notice a neutral temperature dependence with zero gain occuring near 700 K or 800 K, and 5-percent absorption near 900 K (cf. Figs. 2 and 4). This suggests that two different mechanisms are at work, one producing the large absorptions at low kT_e and the other, with a "threshold" near 2 eV, producing the population inversion at higher kT_e.

With the relation between E/N and drift velocity w given by Fig. 6, we can continue the analysis one step further by using the equation

$$J(0) = n_e e w \tag{5}$$

in order to calculate the electron density n_e at the axis of the discharge tube. Using the relation between axial current density $J(0)$ and the total discharge current I, which was derived above, we then obtain the relation

$$n_e = 0.739 I/ewR^2. \tag{6}$$

The values of w are to be taken from Fig. 6.

The partial inversion occurring when rotational levels are in collisional equilibrium has been treated thoroughly in the literature [15]. Here we derive an expression for the

population-inversion density for the specific levels involved in the H_2O-laser emission. We denote the population densities in the specific lower and upper levels as ρ_1 and ρ_2, respectively, and the total vibrational-population densities in the $2\nu_2$ and ν_3 levels as N' and N'', respectively. Since we assume the rotational population within a given vibrational state to be in collisional equilibrium at the gas temperature T, we can use Boltzmann factors to describe the relative population densities in the rotational levels as

$$\rho_i' = \rho_0' g_i' e^{-E_i'/kT} \qquad \rho_i'' = \rho_0'' g_i'' e^{-E_i''/kT}. \tag{7}$$

Also

$$N' = \sum_i \rho_i' = \rho_0' Z' \qquad N'' = \sum_i \rho_i'' = \rho_0'' Z'' \tag{8}$$

where

$$Z' \equiv \sum_i g_i' e^{-E_i'/kT} \qquad Z'' \equiv \sum_i g_i'' e^{-E_i''/kT} \tag{9}$$

are the rotational distribution functions of the lower and upper vibrational states of the laser transition. Using these relations we can express the population-inversion density in the form

$$\rho_2 - \frac{g_2}{g_1}\rho_1 = N'' \frac{g_2}{Z''} F \tag{10}$$

the inversion factor F being given by

$$F \equiv \{e^{-E_2/kT} - Ae^{-E_1/kT}\} \tag{10a}$$

where

$$A = \frac{N'}{N''}\frac{Z''}{Z'}. \tag{10b}$$

If the pumping is accomplished by electron impact, then source terms are of the form $n v_e \sigma$ [X], where X is the, at this point unspecified, target molecule. The dominant losses are due to the de-excitation or excitation transfer during collisions with neutrals and are, therefore, of the form $\nu_{de}N$. In steady state we thus have the equations

$$N' = \frac{n_e v_e}{\nu_{de}'} \sigma_{01}(i)[X_i] \qquad N'' = \frac{n_e v_e}{\nu_{de}''} \sigma_{02}(i)[X_i]. \tag{11}$$

The ratio of partition functions Z''/Z' can be written in terms of the rotational constants to fairly good precision [16]. The gas-temperature dependence then cancels in the ratio so that Z''/Z' is indeed a constant. The rotational constants of interest are not known, but by comparison with those of other molecules we can judge that the ratio $Z''/Z' > 1$, but probably only by a few percent. Thus the value of A is approximately equal to the product of the ratios ν_{de}''/ν_{de}' and σ_{01}/σ_{02}. Due to the difference in the rotational energies $E_2 = 653\ \text{cm}^{-1}$ and $E_1 = 900\ \text{cm}^{-1}$ of the upper and lower levels of the 28-μm transition, a partial inversion can occur even though the total vibrational populations N' and N'' are uninverted (i.e., even when $A > 1$). The temperature dependence of the inversion factor F for several values of A is shown in Fig. 7.

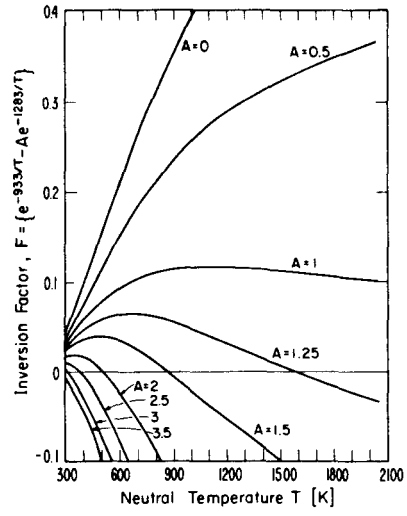

Fig. 7. The inversion factor F of (10a) versus the neutral water-vapor temperature for various values of the parameter A of (10b).

We can also relate the gain per unit path length to the population-inversion density, this time using the equation [17]

$$G = 0.94\left(\rho_2 - \frac{g_2}{g_1}\rho_1\right) A_{21}\lambda^2/8\pi c\Delta(1/\lambda). \tag{12}$$

The linewidth $\Delta(1/\lambda)$ is the Doppler width (FWHM), which for our conditions is approximately $1.9 \times 10^{-3}\ \text{cm}^{-1}$. Using Benedict's value [2], $A_{21} = 6\ \text{s}^{-1}$, and a peak gain of 6×10^{-4} cm^{-1} (6-percent m^{-1}) for the 9.5-mm-bore gain tube, we calculate for the required inversion density, $\rho_2 - \rho_1 g_2/g_1 \simeq 2 \times 10^{10}\ \text{cm}^{-3}$.

Can we now obtain this required inversion density by using appropriate values in (10)–(10b)? We will check each of the four mechanisms to see if sufficient density N'' can be maintained. Using the values $g_2 = 2J_2 + 1 = 13$ and $Z'' \cong Z = 168(T/300)^{3/2} \cong 1000$ [11], we see from (10) that a value of $N''F \simeq 1.5 \times 10^{12}\ \text{cm}^{-3}$ is required. Since mechanisms A), B), and C) are controlled by electron-impact excitation we use (11) in the form

$$N'' = \frac{n_e N}{\nu_{de}''} k_{02} \frac{[X]}{N}$$

where

$$k_{02} = v_e \sigma_{\max} \int_0^\infty \frac{\sigma(v)}{\sigma_{\max}} f(v)\, dv. \tag{13}$$

For the 9.5-mm-bore gain tube at peak gain ($p = 1.6$ torr, $I = 0.14$ A) we calculate $N = 2.4 \times 10^{16}\ \text{cm}^{-3}$ and use the electron density $n_e = 25.6 \times 10^{10}\ \text{cm}^{-3}$ from (6), $\nu_{de}''/N = 8 \times 10^{-12}$ $\text{cm}^3\ \text{s}^{-1}$ at $T = 1000$ K [18], and $v_e = 10^8\ \text{cm} \cdot \text{s}^{-1}$, corresponding to $kT_e = 2.7$ eV.

Cross sections having the desired electron-energy threshold near 2 eV have been observed in several gases for vibrational excitation by electrons through intermediate negative-ion states. The cross section for the vibrational excitation of H_2 through compound negative-ion formation has been measured to peak at a value of $0.4 \times 10^{-16}\ \text{cm}^2$ [19]

TABLE II
ESTIMATES OF N'' AND $N''F$ FOR THERMAL EQUILIBRIUM AND FOR THE VARIOUS PUMPING MECHANISMS A)–D) USING EQUATIONS (13)–(15)

Mechanism	$N''[10^{12}\ cm^{-3}]$	A	$N''F[10^{12}\ cm^{-3}]$
Needed for 6-percent-m^{-1} gain			1.5
Thermal 1000 K	90	2.4	−30
Thermal 900 K	40	2.6	−13
A) electron excitation of H_2O	200	(1)	+25
B) vibrational transfer $H_2 \rightarrow H_2O$	86 $[H_2]/N$	(1)	10 $[H_2]/N$
C) recombination	0.68	(1)	0.08
D) reaction (2)	0.7 $[H_2]/N$	(1)	0.08 $[H_2]/N$
B) vibrational transfer $OH \rightarrow H_2O$	0.7 $[H_2]/N$	(1)	0.08 $[H_2]/N$

Note: Parentheses indicate assumed values.

for an electron energy of about 3 eV. Although the cross sections for water have not been measured, experiments on other molecules, such as CO, indicate peak cross sections of order 10^{-16} cm^2 [20]. Furthermore, the energy of the H_2O^- complex has been estimated [21] to be 1.8 eV above the ground state of H_2O, thus allowing a proper threshold behavior. The integral in (13) for H_2 has a peak value of 0.67 near $kT_e = 1.8$ eV and is > 0.62 between $kT_e = 1.2$ and 2.7 eV. The same value has been used for H_2O in the absence of any direct measurements.

Now, assuming thermal equilibrium between the populations of the ground state and the vibrational states, we can calculate N''/N and also $A = N'/N''$. The resulting values of N'' and $N''F$ for two different gas temperatures in the 9.5-mm gain tube are given in Table II. The other entries in the table give the corresponding values for the different excitation mechanisms. For electron recombination, mechanism C), the pumping rate is given by αn^2, which is balanced by $\nu_{de}''N''$, so that instead of (13) we use

$$N'' = \alpha n^2/\nu_{de}''. \tag{14}$$

For mechanism D) the pumping rate is of the form k [OH] $[X]$, so that instead of (13) we obtain

$$N'' = k_L[OH][H_2]/\nu_{de}'' \tag{15}$$

for reaction (2). Using the rate coefficient $k_L = 3.6 \times 10^{-11} e^{-2600/T}$ suggested by Baulch [22], the value in Table II is obtained. The ratio $[H_2]/N$ was not measured, but arguments based on the continuity equations for OH, H, and H_2 indicate a value in the region of 1–10 percent. Finally, vibrational-excitation transfer from OH to H_2O, suggested by Bugayev [23], must be considered. In our discharge the major source term for OH is by electron-impact dissociation of H_2O. Assuming that every OH is produced in the 1st vibrational state and that all this vibrational excitation is transferred to $H_2O(\nu_3)$, we can then equate the OH $\rightarrow H_2O$ vibrational pumping rate to the OH source function. Since the [OH] seems to be controlled by losses due to (2), we see that the maximum expected values of N'' and $N''F$ should be about the same as for mechanism D). Vibrational excitation by direct electron impact on OH with subsequent excitation transfer to H_2O would be less important due to the low density of OH.

Comparison of the values of Table II allows us to conclude that appreciable contributions from mechanisms C) and D), as well as B) for OH→H_2O, are very unlikely. However, mechanism B) for vibrational-excitation transfer from H_2 to H_2O could be important, provided that $[H_2]/N \gtrsim 0.15$, and that A for this mechanism is not too high. This may be the mechanism responsible for the increase in laser output when H_2 is added.

Considering the possible importance of H_2 in pumping the laser transition by vibrational-excitation transfer, several experimental observations on the 59-mm-bore laser are of importance at this point.

1) The addition of H_2 caused an increase in gain and hence in laser output. Such behavior has been reported by several previous workers [24].

2) The addition of fairly small amounts of H_2 reduced the concentration of OH. Here, small means that the added $[H_2] \ll [H_2O]$. This effect implies that H_2 either controls the loss of OH [as by reaction (2)] or begins to control it at only slightly higher H_2 densities than those present in a pure H_2O discharge.

3) The addition of fairly small amounts of D_2 lowered the laser output.

4) The addition of NH_3 in small amounts produced a 25-percent increase in laser output. Larger amounts led to a reduction in laser output. The introduction of various electronegative gases produced strong quenching of the laser action.

Observations 1) and 2) are consistent with laser pumping due to either mechanism B) or mechanism A), with B) becoming important at the higher H_2 concentrations. These observations also argue against any important contribution due to OH→H_2O vibrational transfer. Since D_2 will be dissociated by electron impact, resulting in large amounts of atomic deuterium, and since the reactions

$$H + D_2 \rightleftarrows HD + D$$

$$H_2 + D \rightleftarrows HD + H$$

have large rate coefficients [25], we then expect a reduction in the H_2 concentration when D_2 is added. Some conversion of H_2O to HDO should also occur, but more slowly and with less percentage reduction in H_2O than for H_2. Observation 3) therefore suggests that mechanism B) contributes appreciably to the inversion.

Finally, the increase in laser output when NH_3 is added may be due to an increase in the H_2 concentration with a corresponding increase in the pumping by mechanism B). The addition of small amounts of electronegative gases quenched the lasing, probably because the formation of negative ions would either reduce the electron density or require the dissipation of more power to maintain the discharge, thus increasing the neutral gas temperature.

IV. Conclusions

We have seen that the gain map (Fig. 2), when compared with the E/N and neutral gas temperature maps (Figs. 4 and 5), indicates two regions of distinct behavior. When E/N is high ($kT_e \gtrsim 2$ eV) appreciable gain occurs which is very sensitive to the electron temperature. This suggests electron-impact excitation through an intermediate negative-ion state, either H_2O^- or H_2^- [mechanism A) or B)]. A value of $A \gtrsim 1.2$ would be needed in the inversion factor in order to explain this gain. For lower E/N ($kT_e < 2$ eV), a large absorption is noticeable and is strongly correlated with the neutral gas temperature. The behavior in this second region is due to the thermal population of the $2\nu_2$ and ν_3 vibrational levels, thus providing a high absorption which must be overcome by the gain pumping mechanisms. Only mechanism A) seems sufficiently strong to overpower this absorption, which it does only marginally. Once the absorption is overcome, the contribution of vibrational-excitation transfer from H_2 to H_2O may be important in increasing the gain. We cannot distinguish between mechanisms A) and B) with any degree of certainty, but the observations suggest that if B) is not important in the case of pure H_2O, it becomes important when even small amounts of H_2 are added to the discharge.

Finally, numerical estimates allow us to rule out mechanism C), electron–ion recombination, and mechanism D), chemical reactions involving OH, as important pumping processes.

As has been suggested previously [4], the enhancement observed when He is added to the discharge is due to a lowering of the neutral gas temperature. Not only is the thermal conductivity of He much higher than that of water vapor, but also the power input per unit length, measured in this experiment, is lower during optimum operation with a He–H_2O mixture. Apparently, the production of ionization is more efficient in this case. The production of H_2O^+ proceeds not only by electron impact on H_2O and by charge transfer with He^+, but also by reactions involved with electronically excited He

$$He^* + H_2O \rightarrow He + H_2O^+ + e.$$

Thus more ionization is produced with less power. However, rather than increasing the active pumping mechanism which occurs for $kT_e \gtrsim 2$ eV, the major effect of He is probably through a reduction in the large absorption due to thermal excitation. The complexity involved in these competing mechanisms qualitatively explains the large variation in enhancement ratios (power for the mixture/power for pure H_2O) seen in this and in previous work [24]. In this present experiment, He-enhancement ratios varied from 1.25 to 3 or 4, and H_2-enhancement ratios from less than 2 to more than 6 in the 59-mm-bore laser. The optimum ratio of He to H_2O pressures was found to lie between 3 and 6, with the enhancement not very sensitive to the exact value. The total pressure was about 1.2–1.8 torr, the partial pressure of H_2O being slightly less than the optimum for pure H_2O. The addition of H_2 to the H_2O–He mixture generally produced a further enhancement which was also quite variable, ranging from a factor of 2 or more down to no noticeable increase.

A more definitive study of the H_2O laser would require measurements of the densities of the neutral species present as well as some better knowledge of the tail of the electron-velocity distribution. Hopefully, some of the needed vibrational excitation and de-excitation cross sections in H_2O, particularly the excitation through negative-ion states, and the de-excitation collision frequencies, will soon be measured.

The observed dependence of gas density and gain on the tube diameter (Fig. 3) suggests that significantly higher power can be expected from small-bore H_2O lasers. A waveguide H_2O laser at 28 μm is therefore a distinct possibility.

Acknowledgment

The author wishes to thank J. C. Bennett for his able assistance with the task of accumulating the gain and electric-field measurements and in the processing of some of these data, Dr. A. V. Phelps for several very helpful discussions, and Dr. C. J. Howard for information concerning certain aspects of the neutral chemistry.

References

[1] A. Crocker, H. A. Gebbie, M. F. Kimmitt, and L. E. S. Mathias, "Stimulated emission in the far infra-red," *Nature*, vol. 201, pp. 250–251, 1964.

[2] W. S. Benedict, M. A. Pollack, and W. J. Tomlinson, III, "The water-vapor laser," *IEEE J. Quantum Electron.*, vol. QE-5, pp. 108–124, Feb. 1969.

[3] W. J. Sargent, Z. Kucerovsky, and E. Brannen, "Excitation processes and relaxation rates in the pulsed water vapor laser," *Appl. Opt.*, vol. 11, pp. 735–741, 1972.

[4] a) J. P. Pichamuthu, J. C. Hassler, and P. D. Coleman, "Excitation mechanism of the water-vapor laser," *Appl. Phys. Lett.*, vol. 19, pp. 510–512, 1971.
b) J. P. Pichamuthu *et al.*, "Gas temperature measurement in pulsed H_2O laser discharges," *J. Appl. Phys.*, vol. 43, pp. 4562–4565, 1972.
c) J. P. Pichamuthu *et al.*, "The role of helium in the H_2O laser," *IEEE J. Quantum Electron.* (Corresp.), vol. QE-9, pp. 244–245, Feb. 1973.

[5] K. M. Evenson, private communication.

[6] A. V. Phelps suggested this possibility.

[7] J. Schutten, F. J. deHeer, H. R. Moustafa, A. J. H. Boerboom, and J. Kistemaker, "Gross- and partial-ionization cross sections for electrons on water vapor in the energy range 0.1–20 KeV," *J. Chem. Phys.*, vol. 44, pp. 3924–3928, 1966.

[8] R. A. Fluegge, "Ion-Molecule reactions in alpha-particle-irradiated methane and water vapor," *J. Chem. Phys.*, vol. 50, pp. 4373–4380, 1969.

[9] M. T. Leu, M. A. Biondi, and P. Johnsen, "Measurements of the recombination of electrons with $H_3O^+ \cdot (H_2O)_n$-series ions," *Phys. Rev. A*, vol. 7, pp. 292–298, 1973.

[10] P. F. Bird and G. L. Schott, "Quantative line absorption spectrophotometry: Absorbance of the OH radical near 3090 Å," *J. Quant. Spectrosc. Radiat. Transfer*, vol. 5, pp. 783–811, 1965.

[11] D. M. Gates, R. F. Calfee, D. W. Hansen, and W. S. Benedict, "Line parameters and computed spectra for water vapor bands at 2.7 μ," NBS Monograph 271, 1964.

[12] *Handbook of Chemistry and Physics*, 53rd ed., Chemical Rubber Co., 1972, p. E-3.

[13] P. Kebarle, S. K. Searles, A. Zolla, J. Searborough, and M. Arshadi, "The solvation of the hydrogen ion by water molecules in the gas phase," *J. Amer. Chem. Soc.*, vol. 89, pp. 6393–6399, 1967.

[14] A. V. Phelps and R. S. Cohen, private communication.
[15] J. C. Polanyi, "Vibrational-rotational population inversion," *Appl. Opt. Suppl.*, vol. 2, pp. 109–127, 1965.
[16] G. Herzberg, *Infrared and Raman Spectra*. Princeton, N.J.: Van Nostrand, p. 506.
[17] Derivable from A. Yariv, *Quantum Electronics*. New York: Wiley, 1967, p. 210, Eq. (13.3-15).
[18] K. Yamada and Y. Fujii, "Ultrasonic attenuation and relaxation times in water vapor and heavy-water vapor," *J. Acoust. Soc. Amer.*, vol. 39, pp. 250–254, 1966.
[19] F. Linder and H. Schmidt, "Rotational and vibrational excitation of H_2 by slow electron impact," *Z. Naturforsch. A*, vol. 26, pp. 1603–1617. 1971.
[20] H. Ehrhardt, L. Langhans, F. Linder, and H. S. Taylor, "Resonance scattering of slow electrons from H_2 and CO angular distributions," *Phys. Rev.*, vol. 173, pp. 222–230, 1968.
[21] C. R. Claydon, G. A. Segal, and H. S. Taylor, "Theoretical interpretation of the optical and electron scattering spectra of H_2O," *J. Chem. Phys.*, vol. 54, pp. 3799–3816, 1971.
[22] D. L. Baulch *et al.*, "High temperature reaction rate data #2," Dept. Phys. Chem., Univ. Leeds, Leeds 2, England, Nov. 1968.
[23] V. A. Bugayev, "The oscillation mechanism of a submillimeter laser using water vapor," *Radio Eng. Electron. Phys.*, vol. 14, pp. 979–980, 1969.
[24] a) A. F. Krupnov, V. A. Skvortsov, and L. A. Sinegubko, "The effect of gas impurities in the operation of H_2O and D_2O submillimeter lasers," *Radio Eng. Electron. Phys.*, vol. 14, pp. 1170–1171, 1969.
b) S. F. Dyubko, V. A. Svich, and R. A. Valitov, "Hydrogen as a buffer gas in a submillimeter water-vapor laser," *Sov. Phys.—Tech. Phys.*, vol. 13, pp. 1596–1597, 1969.
c) W. J. Sarjeant and E. Brannen, "Enhancement of laser action in H_2O by the addition of helium," *IEEE J. Quantum. Electron.* (Corresp.), vol. QE-5, pp. 620–621, Dec. 1969.
[25] G. Boato *et al.*, "Homogeneous exchange reaction between hydrogen and deuterium," *J. Chem. Phys.*, vol. 24, pp. 783–791, 1956.